Modelling and Sizing of NaS Battery Energy Storage System for Extending Wind Power Performance in Crete Island

E.M.G. Rodrigues[a], G.J. Osório[a], R. Godina[a], A.W. Bizuayehu[a], J.M. Lujano-Rojas[a], J.C.O. Matias[a], J.P.S. Catalão [a,b,c,*]

[a] *University of Beira Interior, R. Fonte do Lameiro, Covilha, Portugal*
[b] *INESC-ID, R. Alves Redol, Lisbon, Portugal*
[c] *IST, University of Lisbon, Av. Rovisco Pais, Lisbon, Portugal*

Abstract

Crete Island is rich in renewable energy resources such as wind and solar. Likewise other European territories, renewable sources already are being explored for power production. Currently a large amount of wind energy on Crete is curtailed during certain daily periods as a result of reduced demand and minimum operating levels on thermal generators. Reducing wind power curtailment magnitude requires additional sources of flexibility in the grid, and electric energy storage is one of them. This paper address wind generation curtailment minimization through the storage of wind energy surplus. Sodium Sulfur (NaS) battery modelling is used in this study in order to shift wind generation from off-peak to on-peak through a technical-economic analysis, considering the total annualized cost of the storage system and the wind power curtailment based on an annual basis. The obtained results are based on real data, which includes Crete Island demand, renewable and conventional power generation.

Keywords: Wind farm; Curtailed wind energy; Battery energy storage system; Energy capacity.

1. Introduction

Wind curtailment is not anymore an isolated event or with low probability of occurrence in power systems. Progressive integration of large renewable capacity in the grid management has become a serious matter to be taken into consideration. Modern grid codes give direct priority dispatch for renewable generation. However, to maintain the power grid operation secure and dependable, security based limits are locally imposed by grid operators. As a result, renewable generators are obliged to cut some of their outputs to fulfil security limit's rules. By definition, wind curtailment is a deliberate decrease in wind power output ordered by the system operator to avoid the risk of instability on the grid from non-synchronous generation as well as other motives such as managing grid stability and reserve requirements [1] [2] [3]. As wind and solar penetration is growing, curtailment rates are expected to increase.

* Corresponding author at: University of Beira Interior, R. Fonte do Lameiro, 6201-001 Covilha, Portugal. Tel.: +351 275 329914; fax: +351 275 329972.
E-mail address: catalao@ubi.pt (J.P.S. Catalão).

The dispatch down from wind farms is an observed global phenomenon in several regions where wind power integration is fast and significant. In Spain, for example, approximately 315200 MWh of wind energy were curtailed in 2010 [4]. Similarly, in the USA Texas state, vigorous curtailment actions have been taken by the grid operator, wasting 17.1% of possible wind generation on an annual basis from 2007 to 2012 [5]. Transmission constraints in Chinese power grid has also led to significant dispatch down actions and incurring in generation losses.

On the other hand, only few exceptions have been reported without employing curtailment measurements. For example in Denmark in 2012 there was a record of 30.1% of renewable electricity consumption with an insignificant wind generation losses due to electric power transit agreements with neighbouring countries. Whenever wind production exceeds consumption the surplus is sent to hydro based systems in Norway and Sweden. In other countries like Portugal wind curtailment is not authorized due to legislation restriction, except when originated from technical problems.

Dispatch down events penalizes wind farm owners by causing profit losses. Moreover, these practices are in counter-cycle with the global world trend of reducing greenhouse gas emissions.

Efforts to mitigate curtailment procedures involve integrating supplementary sources of flexibility in the grid. Those can be divided into three categories: 1) network reinforcement, 2) improved utilization of the existing network infrastructure, and 3) coordination between wind generation and electric energy storage resources [6].

Storage represents a reservoir of energy for periods of low or even absent wind generation by capturing excess energy when a surplus is available. Coupling wind generation and storage is now being seen as credible to improve combined performance in the medium term. Storage systems coupled to wind turbines can cover different functionalities. One way of solving wind output fluctuations relies on adding storage based on battery devices for smoothing power output [7], instead of using fast-acting dispatchable sources such as hydro generators or natural gas turbines that can raise costs of more wind integration [8]. Storage systems can have other functions such as providing frequency response capability from wind farms among others. Battery storage schemes may also provide more than one purpose such as smoothing output combined with power balance support [9].

Provision for other ancillary services traditionally handled by conventional generation such as load following, reserve capacity or voltage support has been reported feasible and effective by using different battery technologies [10] [11].

However, many technical, economic and operational challenges have to be solved before storage devices installation takes place at large-scale. For example, determining cycle-to-cycle round-trip efficiency is critical for battery health and life span estimations, which when poorly understood lead to over-optimistic calculation of storage operational costs [12]. Other forms of energy storage are in advanced stage of development and involving pilot-projects or already in real-world usage namely flywheels and supercapacitors for grid power quality control and compressed air plants along pumped-storage hydroelectricity for long-term storage applications.

Crete Island is a singular case for wind curtailment studies. The average annual wind power penetration is already high and imposing serious challenges to the grid operator. Installed wind power production has been under-explored in order to accomplish safe system operation levels in terms of reserve margins, voltage profiles and dynamic stability. Therefore, wind curtailment events are significant and recurrent.

One way to store energy is with NaS batteries, which use molten sodium and sulfur as electroactive materials. The NaS battery is able of both high energy and high power operation, being limited mostly by thermal dissipation [13].

In [14], an analysis and investigation of operating methods and costs of an independent microgrid is proposed by incorporating a NaS battery and an energy storage system using organic hydrides. A proposal of a stochastic model predictive control scheme for wind farm dispatching employing probabilistic wind power forecasts with NaS battery energy storage is made in [15], and all this with the use of real data that were obtained in the real operation of a wind farm. The ability of the Energy Storage Systems (ESS) to increase the amount of wind energy accepted onto a network is assessed in [16] over a range of roundtrip storage efficiencies and an analysis is then conducted to determine the cost of energy produced through the hydrogen-based and NaS ESS for a number of scenarios. In [17] field results are presented and, like in [13], the ability of the NaS battery to limit the ramp-rate of the wind farm output is evaluated and the capability and the value of the NaS battery in shifting wind-generated energy from off-peak hours to on-peak hours are assessed.

A joint and disjoint operation of wind power plant (WPP) and NaS plant with reference to expected profit maximization and WPP forecasting error compensation by NaS Plant is proposed in [18]. In [19], a study that critically examines the existing literature in the analysis of life cycle costs of utility-scale electricity storage systems is carried out, including NaS, providing an updated database for the cost elements. In [20], the performance of the NaS storage is statistically evaluated in a stochastic framework where day-ahead forecast errors are modeled with an autoregressive model. The aim of [21] is to present the current situation of the energy storage and also to propose applications of a specific NaS battery for wind farms in Hungary. In [22], an energy storage system sizing study for a high-altitude wind energy system based on several batteries including NaS is presented.

This paper presents comprehensive numerical results and analysis quantifying the ability of NaS battery energy storage to reduce global wind power curtailment levels in Crete's grid. The application of NaS is proposed to shift the wind generation from off-peak to on-peak. A technical-economic analysis is performed in order to get optimal ratio of storage as a global figure for the Crete system. In this regard, the sizing of NaS energy storage resources considers the total annualized cost of the storage system and the wind power curtailed on an annual basis. Simulation results rely on Crete's grid generation and on demand figures reported to year 2011. Field figures concerning conventional generation, load demand, wind power generation and curtailed wind power on an annual basis were obtained under the Singular Project [23]. The remainder of the paper is organized as follows: in Section 2, the real generation and energy consumption profile of Crete's power grid is described; Section 3 provides NaS battery characterization and cell electrical modelling. Section 4 is dedicated to the battery storage control strategy. Section 5 present computational simulations and sizing results of battery energy storage system. Finally, Section 6 summarizes the findings of this work.

2. Crete power system

Among Greece's islands Crete has the largest autonomous isolated power system. Most of electricity production still relies on burning fossil fuels. Before the current renewable trend, wind farms in Crete started being installed in the 80s, having now several installations across the island and with a total installed capacity of 170 MW. More recently, photovoltaic parks were introduced with a combined power output of 65 MW. Conventional generation infrastructure in Crete can be seen in [24].

Conventional power stations range from steam turbines powered generation to combined-cycle gas-fired production station. Diesel and gas turbines have a share over 60% which promotes considerable flexibility when it comes to respond to demand needs. This group of generators may operate within an extended range of power output set points. In fact, diesel machines are able to lower the output below to 1/3 of its rated power, while gas turbines reveal a wider service range which in some cases are extremely low as 1/6 of nominal power specification. Wind generation resources are distributed over 26 farms. Despite increasing integration of photovoltaic energy its role in the present study is not relevant. The outcome from this resource is mostly generated on domestic house roofs which are a large number of installations often equipped with very low power rating inverters. Yet, low end inverters do not offer smart management capabilities for the domestic market. Therefore, since they act as isolated generators by injecting all the energy available in the PV panels the system operator can't influence their operation. In this paper, load and wind power outputs as well as fossil fuel based electricity production are analysed, considering one year of hourly real data gathering along 2011. The collected information not only contains the sum of individual conventional generating units, but also each wind farm connected to the Crete grid.

Fig. 1a depicts daily average load demand and it is almost constant during the first quarter of 2011. Close to May, power demand starts to increase and reaches its peak between July and August. This seasonal behaviour is easy explained since in summer months Crete Island receives a lot of tourists. Thus, energy needs boosts as high as one third in this period of the year. As expected, thermal power generation covers the majority of island power needs, the remaining being fulfilled by solar and wind power installations. While demand data demonstrate a continuous variation on its profile, a very erratic wind production profile makes clear that wind resource is highly intermittent in intensity and occurrence terms.

Consequently, it is hard to match its production to satisfy power balance requirements which leads to periodic wind energy curtailment actions. Fig. 1b reveals that curtailment practice was used repeatedly in the course of the year.

Next, a different perspective is presented by combining daily minimum and maximum variation with average value: on load demand (Fig. 2a) and on theoretical wind generation (Fig. 2b).

"See Fig. 1 at the end of the manuscript".

"See Fig. 2 at the end of the manuscript".

Load demand variation appears to be very constant over the entire year. However, the level of increase from minimum to maximum is considerable high. On a winter day we have a minimum consumption around 200MW and a maximum over 400MW. At summer in a peak day consumption oscillates between 300MW and 550MW. Fig. 2b clearly shows that the wind generation profile is by nature erratic and moving from zero generation to a maximum output. Unlike noticed on the load demand figure wind power production has a highly variable generation range. This behaviour is even more intense for winter and autumn months whose minimum falls often to zero, while during the hottest months zero generation is less frequent. An improvement on minimum generation towards summer months can also be noticed.

Previous figures have highlighted key aspects of load and wind generation potential in Crete Island. Despite their importance for the present study their contribution is not enough to evaluate battery based energy storage potential. A further analysis has to be made on how much energy is curtailed on known and fixed time frames of the year. Having this in mind, it was decided to compute power system energy transit by providing satisfactory resolution to identify trends on Crete system.

Fig. 3 shows the energy delivered through conventional generation along with the amount of energy from solar and wind sources on a monthly basis. Included in each balance is also shown the theoretical wind production and the amount of wind curtailment as a percentage rate.

The gross wind energy generation was 741.7GWh in which 176.4 GWh refer to wind power curtailment. The amount of dispatch-down has represented for 2011 almost 24% of total available energy from wind resources of Crete's power system and was mostly concentrated in coldest months.

The level of curtailment in this period may be explained by two reasons: one can be immediately seen by observing the figure that load demand is lower than during summer and the second that there is evidence that minimum generation levels on conventional generation compared to the amount of demand may have triggered additional wind curtailment. As the summer approaches the dispatch-down of wind shows a clear tendency to be less energetic due to an apparent correlation with an increasing demand by this time of the year. A deeper characterization may be conducted by sampling two typical months, whereas one is at winter peak and the other coincides with the highest demand in summer.

Fig. 4 shows wind curtailment profile during three different periods of the day, respectively for January and August months.

In January, wind revealed to be more active at night and exceeding several times by a factor of two the level of wind curtailment when compared to the rest of the day. This is a clear sign that during winter season the installed wind capacity is in excess when loads are low. Therefore, thermal units are pushed down against their minimum operating constraints.

"See Fig. 3 at the end of the manuscript".

"See Fig. 4 at the end of the manuscript".

However, in August, wind curtailment profile shows an inverse tendency. Curtailment peaks are stronger during the day than during the night. This additional curtailment at peak hours has the potential to be easily recovered instead of wasted since it happens when load is high and as a consequence some of the flexible thermal generation may be turn down.

3. Modelling of electric energy storage system

3.1 NaS battery technology

This battery type uses molten sodium for the anode and liquid sulfur for the cathode. The positive and negative terminals are separated by a beta-alumina solid electrolyte. Initially developed for electric vehicles by Ford Motor Company, its evolution has been shifted to address power grid applications. The technology became commercial in Japan and presently several real scale facilities are operating as demonstration units in countries like the United States.

NaS battery systems show important features when compared to others chemical batteries. They offer a good balance between power capability and energy density ratio. In terms of power capability, they can provide single continuous discharge at power rating during all discharging period, or if necessary the battery energy can be released in a shorter discharge period. It has the ability to release five times its nominal power rating in very short times [25].

In turn, NaS round-trip efficiency reaches 80% and self-discharge effect is less pronounced, which results in long time storing capability. In addition, its discharge capacity over a long-term cycling operation is significant. If operated at 100% depth of discharge, NaS battery can retain full battery capacity over 2500 cycles, while at 50% of full discharge the life cycle number rises up to 7000 [26].

Finally, this technology does not require consumption of especial materials since it uses low cost raw materials. To promote sodium ions movement through the electrolyte the battery must run at a sufficiently high temperature.

Otherwise, it is not possible to keep active electrode materials in a molten state. Therefore, a mandatory condition for ensuring good ionic conductivity is to keep the temperature at least at 300ºC to maintain both electrodes in liquid state. Usually the operating temperature should be within the range of 290-390ºC [13].

These batteries are being commercialized to target large electric energy storage. In effect, NaS storage commercial units provide several MW power loads and MWh order capacities. Due to their power ratings, they are tailored for utility scale applications, providing a broad range of services for grid performance improvement as well as to support renewable power generation [27].

3.2 NaS cell model

A battery device relies on electrochemical reactions to store electric charges. When connected to an electric load it has the ability to release energy (discharge mode) or to receive it from an external source (charging mode). To analyze NaS battery cell an electric equivalent circuit is used. Although this approach has low complexity it provides good information about battery I-V characteristics modelling [28]. A generic model consists of an ideal DC electric source, representing an open circuit voltage in series with one or more resistances that model internal parasitic effects linked with electrolyte, plate and fluid resistance. Battery types as well as the parameters available for its description along with the accuracy level required determine the complexity of the adopted electric model. For example, a more detailed model may include different resistive paths for taking into account differences in the charging/discharge processes.

Other types of modelling could be employed such as those supported on fundamental physical and electrochemical processes description instead of the electric circuit approach. Those alternatives require more computational resources. However, they can be very effective in identifying cell performance constraints during cell design optimization [29].

Evaluating NaS battery storage system performance requires the characterization of the model's electric parameters as a function of the battery charge state. Typically, all battery technologies show a strong relationship with the state of charge (SOC) level, which is the percentage of the battery's rated capacity that is available at a given time. Equally, depth of discharge (DOD) ratio is also an equivalent way to quantify the electric charge available by withdrawing the minimum SOC from 100%. It implies that if SOC value is known then the battery electric state variables are also known.

Four parameters are used to model the electric battery operation: open circuit voltage (V_{oc}), charging resistance (R_{ch}), discharging resistance (R_d) and supplementary internal resistance (R_{lc}) due to the cycling activity of charging and discharging.

In this paper, real data provided under the Singular project allowed us to gather up a set of physical data in order to model in electrical terms the main NaS cell parameters.

Fig. 5 presents the characteristics of open circuit voltage V_{oc} via battery DOD. Fig. 6 shows internal resistances R_{ch} and R_{dis} relationship to battery DOD and room temperature, while R_{lc} variation as a function of charge-discharge cycle number (N) is shown in Fig. 7.

"See Fig. 5 at the end of the manuscript".

"See Fig. 6 at the end of the manuscript".

"See Fig. 7 at the end of the manuscript".

In Figs. 6 and 7, it can be seen that room temperature has a visible effect on the evolution of internal ohmic losses concerning the NaS cell charge/discharge process, especially in certain ranges of battery DOD. From conversion efficiency point of view (minimizing internal ohmic power losses), it seems adequate to operate NaS battery within a 20-70% range. However, this has necessary implications on size specification since some of the rating capacity will not be used in a real application.

Voltage at battery output terminals (V_{bat}) depends on operation mode. For discharging state, it can be expressed as:

$$V_{bat} = V_{oc} - R_{dis}I_{bat} - R_{lc}I_{bat} \quad (1)$$

and for charging mode as:

$$V_{bat} = V_{oc} + R_c I_{bat} + R_{lc}I_{bat} \quad (2)$$

where both R_{dis} and R_{ch} depend on battery DOD and can be approximated by polynomial regression of degree 9 and 10, respectively:

$$R_{dis} = a + bDOD^2 + cDOD^3 + dDOD^4 + eDOD^5 + fDOD^6 + gDOD^7 + hDOD^8 + iDOD^9 \quad (3)$$

$$R_{ch} = a + bDOD^2 + cDOD^3 + dDOD^4 + eDOD^5 + fDOD^6 + gDOD^7 + hDOD^8 + iDOD^9 + jDOD^{10} \quad (4)$$

Curve fit coefficients are shown in Tables 1 and 2. The R_{lc} life-cycle resistance, which is updated as the battery cycle number increases, has the following expression and can be observed in Fig 8:

$$R_{lc} = 0{,}0108N^{0.4844} \quad (5)$$

while V_{oc} experimental data changing with DOD is expressed as:

$$V_{oc} = \begin{cases} 2.076\,, & DOD \leq 0.56 \\ 2.076 - 0.00672DOD\,, & DOD > 0.56 \end{cases} \quad (6)$$

"See Table 1 at the end of the manuscript".

"See Table 2 at the end of the manuscript".

"See Fig. 8 at the end of the manuscript".

The capacity value of a new battery does not stay unchanged while the battery is operated over time. The capacity fade depends strongly on the application itself, usage conditions, SOC and temperature [30]. Battery lifetime prediction is critical for the long term energy cost estimation of such projects. A major factor for the battery aging process has to do with the fact of whether the battery is cycled at large DOD amplitudes or, on the contrary, at reduced DOD level. In fact, the cycle counting method is based on the assumption that the charge cycle amplitude determines a certain reduction of battery lifetime.

NaS cycles vs failure data were obtained in [23] and are plotted in Fig 9. This figure relates the number of charge cycles to the life of the battery. The vertical axis determines the number of charge cycles at which, for a specific DOD amplitude, battery capacity falls below 80% of its initial rated capacity.

"See Fig. 9 at the end of the manuscript".

A single exponential curve is used to fit cycles to failure points. Consequently, the NaS lifetime model can be expressed as:

$$N_{cy} = 1.978 \times 10^6 (DOD)^{-1.73} + 3101 \quad (7)$$

4. Battery control

A controller has been implemented with the mission to manage power flow between storage system and the grid. The specific charging and discharging profiles are defined by the controller, which establishes a power reference command P_{ref}. The P_{ref} value depends on wind power generated in excess at a specific instant *j*, battery SOC and rated values for input/output power.

Excess wind power ($P_j^{Exc\,WP}$) is given by:

$$P_j^{Exc\,WP} = P_j^{WG_{Theo}} - P_j^{WG_{Grid}} \quad (8)$$

where $P_j^{WG_{Theo}}$ is the gross wind power at instant *j*, and $P_j^{WG_{Grid}}$ is the net wind power delivered to the grid at instant *j*. In case of $P_j^{Exc\,WP}$ exceeding rated charging power (P_{rated}^{ch}), the storage system controller imposes this nominal figure as P_{ref}. As a result, the difference between $P_j^{Exc\,WP}$ and P_{rated}^{ch} is discarded as effective curtailed wind energy. On the other hand, when $P_j^{Exc\,WP}$ is lower than P_{rated}^{ch}, all surplus wind generation is stored. In turn, P_{ref} for output power is limited to the rated discharge power (P_{rated}^{ch}) of the storage banks. Of course if the available energy is less than the necessary to provide P_{rated}^{ch}, P_{ref} is adjusted to comply with the stored energy.

The energy storage units comprise aggregated battery banks and AC-DC power conversion systems to interface with the grid. Energy counting can be expressed as:

$$E_j = E_{j-1} + P_j^m \Delta t \eta_j^{bat\_m} \eta_j^{conv\_m} \tag{9}$$

where E_j is the energy stored at instant *j*, E_{j-1} is the energy stored at previous instant *j-1*, $P_j^{bat\_m}$ is the storage banks power transit at instant *j*, $\eta_j^{bat\_m}$ is the storage banks efficiency at instant *j*, $\eta_j^{conv\_m}$ is the power converter efficiency at instant *j*, Δt is the period for storage bank operation and the *m* upper index designates battery usage mode (*ch* for charging and *dis* for discharging).

Storage inefficiencies reduce the amount of energy to be effectively stored or released. NaS battery losses model is complex and can have several sources. One way is to approximate battery energy conversion efficiency as:

$$\eta_j^{bat\_dis} = \frac{V_j^{oc} I_j - I_j \left(R_j^{dis} + R_j^{lc}\right)^2}{V_j^{oc} I_j} \quad \text{discharge mode,} \qquad P_j^{dis} < 0 \tag{10}$$

$$\eta_j^{bat\_ch} = \frac{V_j^{oc} I_j}{V_j^{oc} I_j + I_j \left(R_j^{ch} + R_j^{lc}\right)^2} \quad \text{charge mode,} \qquad P_j{}^{ch} > 0 \tag{11}$$

Regarding the conversion efficiency from AC to DC power and vice-versa, it is assumed as constant in both directions and set at 90%. While Eq. 9 is useful as energy counter, it does not provide information about energy storage limits. Thus, in order to not surpass the energy storage system rating, a SOC algorithm has been implemented according to:

$$SOC_j = SOC_{j-1} + \int_0^t \frac{P_j^m \eta_j^{bat\_m} \eta_j^{conv\_m} dt}{E_{rat}} \tag{12}$$

$$0 \leq SOC_j \leq 1 \tag{13}$$

where E_{rat} is the rated energy capacity of the NaS storage unit.

This modelling feature allows the estimation of how much energy is released or stored at any instant t, preventing overcharging events as well as undercharging situations which have consequences in the battery life on long term. Typically, it is desired to confine the SOC of a battery within suitable limits, for example 20% ≤ SOC ≤ 95%. However, to operate the battery continuously and with the smallest size possible the implemented SOC control in this paper does not impose limit restrictions. Thus, complete discharge is permitted.

5.Simulation and Sizing of Battery Energy Storage System

5.1 General considerations

A time-shifting energy strategy is employed to study NaS battery capability in order to reduce wind curtailment.

In this scheme, the electric energy storage system is charged with an excess wind generation, mostly available at night when there are less electric loads connected to the grid and the price of energy is also lower. During the day the charge is released to support the high demand period. In this paper, the scheme is programmed on a daily basis to perform grid support by discharging energy at constant power rating. Therefore, storage discharge duration is estimated by battery bank nominal plate ratings. However, in the present study the storage system discharge mode is set to the maximum time period without violating nominal plate characteristics. Extending to a maximum value has a positive effect by delaying power output response from other conventional sources and giving more flexibility to the grid operator to schedule flexible power plants. Battery operation is configured to perform only a single charge/discharge cycle per day in order to extend the life cycle operation. Daily schedule is fixed on a time basis meaning that start and finish times for each operation mode do not change over the simulated period. Discharge action runs for almost 8 hours covering peak power demand during morning (08.00 AM) until mid-afternoon (03.00 PM). Stored energy is released and controlled to supply constant power output as a function of the 2MW modules connected in parallel which implies nominal power output is given by the modules sum affected to the bank. Whenever the remaining stored energy doesn't allow power injection at nominal rating the output level is updated based on SOC.

Storage system charging mode is initiated during off-peak hours starting at 10.00 PM and remaining that way for 8 hours (Scenario I); on the other hand, an alternative more flexible time-frame scenario is also analysed for battery charging purposes (Scenario II), which means that this scenario is not confined only to off-peak hours. The charging period can be shortened if wind curtailment is enough to charge the batteries completely.

For the present study NaS cells are combined to form a basic storage unit of 2 MW power rating. Each unit comprises 20 batteries connected in parallel mode and each one rated at 50 kW and capable of storing 360 kWh, giving a total of 14.4 MWh as energy rating.

This power/energy rating model is the starting point for building larger generating storage systems, which follow a simple rule of grouping 2 MW power modules in a parallel configuration. A detailed flowchart of the storage system management process and curtailed wind power tracking is provided in Fig. 10.

"See Fig. 10 at the end of the manuscript".

5.2 A technical analysis insight

Choosing an optimal size for the energy storage system requires a clear and detailed identification of services to be provided. Other issues such as expected lifetime service have a strong influence on the storage system energy and power specifications. Accomplishing these requirements depends not only on the charge/discharge cycle control scheme adopted, but also on the power capability of the storage device. Having this in mind, NaS storage system should be able to capture as maximum wind curtailment as possible on a daily basis while at the same time SOC should be close to one unit after every charging period. This requirement implies that the battery storage capacity should not be excessively oversized otherwise some of the rating capacity will be underused.

From power rating point of view storage installations with higher charging power capability have more chances to store wind curtailment peaks. However, the amplitude of these peaks as well as its duration depends not only on meteorological conditions that could provide high wind generation, but also on the period of the day where demand may be low or high.

Fig. 11 shows the storage power rating impact considering a real time series sample of wind curtailment in Crete.

"See Fig. 11 at the end of the manuscript".

It can be seen that successive increase power/capacity ratio offers a better capability to capture excessive wind energy. However, for the largest storage banks a higher power rating capability can only be useful on sporadic and short time periods where the storage potential is higher.

For example, a storage installation of 80MW rating can track the maximum wind curtailment on this time series sample. Therefore, all the curtailment generated will be directed to the battery banks, although usable battery capacity comparatively to its nominal characteristics is low. In turn, the lowest of tested battery banks is clearly insufficient to store the majority of the deployed excess energy as wind curtailment.

Battery banks are rated by the amount of energy that they can store. Since storage banks in this assessment are discharged and charged on a daily basis, usable capacity can be evaluated by checking its value when a charge period comes to an end. Fig. 12 depicts daily stored energy level for three power-to-energy ratio scenarios. In the lowest one, nominal capacity is fully utilized. Between the three scenarios, the largest battery bank stores the highest amount of energy.

"See Fig. 12 at the end of the manuscript".

Yet, by moving from the smallest to the largest installation, usable capacity compared to the maximum available falls from a fully usage condition to a less than 30% of total available capacity utilization level. It is clear that usable capacity allows a better characterization of the storage performance, meaning that energy rating will not improve overall performance beyond a certain level since it is done by oversizing the installation's gross capacity. A better alternative to assess storage performance is through SOC measurements, as it allows a direct quantification of effectively used storage resources compared to the maximum available value.

Fig. 13 gathers data from daily charging throughout the year 2011 where the SOC profile is organized according to the number of occurrences. The lower power to energy ratios are charged mostly closed to their capacity ratings. However, a high usage rate of battery capacity cannot inform by itself how much curtailment is really being stored. On the other hand, bigger battery banks reveal very low SOC rates while intermediate size battery banks show a flatter SOC utilization rate. Therefore, middle size ratings clearly indicate that an optimal storage size relies within this sub-range, allowing maximization of stored wind power surplus.

"See Fig. 13 at the end of the manuscript".

Two merit figures are used to assess both energy and power specifications for the storage system. The first one accounts the accumulated stored energy over wind curtailment data for 2011 and from here now called storage curtailment ratio. The second one refers to the daily average SOC. First, it is considered that the storage charge duration is limited to a time frame of eight hours – starting at 22:00 PM and ending at 6:00 AM (Scenario I).

Fig. 14 characterizes storage performance through the two metrics mentioned previously. The highest ratios show that the wind curtailment capturing capability will stabilize around 60% of total wind curtailment available over the year. Therefore, it defines a theoretical limit for recovering wind curtailment. From SOC perspective, daily usable capacity is distinctly low in this storage size range. In turn, the smallest three battery banks present a storage higher than 70% of nominal energy capacity (4MW/28.8MWh to 16MW/115.2MW), even though at the cost of sacrificing the curtailment storage potential by half.

Since the results demonstrate that there is a significant potential for storing additional wind curtailment, instead of using this limited time frame the charge period was extended outside of off-peak hours in order to further evaluate its impact on the indicators performance. The charging time frame is anticipated to start at 16:00 PM, while the end hour remains the same (Scenario II).

Merit figures values were re-calculated and compared with previous results as shown in Fig. 15. In the upper part of this figure, the storage to curtailment efficiency for both scenarios is illustrated, while in the lower part of the figure the obtained storage increment by switching to the extended charging time frame is noticeable (Scenario II). Storage improvement varies between 8% and 26% which is significant. Further, by comparing storage banks with same size it is also observed an improvement on battery SOC since the extended time frame has moved to the right. Despite the global improvement – usable capacity is still far from the ideal since larger storage systems are not economically attractive and their oversized energy capacity is rarely employed.

However, for example, if a minimum limit of 70% is set as acceptable average SOC, then storage power ratings ranging from 24MW to 40MW stand out. A comparison between these ratings in Scenario II when compared to Scenario I indicates a stored energy gain around 11% for 40MW/288MWh rating. Between all three, this ratting offers a trade-off solution due to its high effective daily energy capacity usage, also allowing an annual wind curtailment recovery ratio above 60%.

"See Fig. 14 at the end of the manuscript".

"See Fig. 15 at the end of the manuscript".

5.3 Technical economic analysis

a) Formulation

Sizing of battery bank is carried out considering the Total Annualized Cost (TAC) of the storage system and the wind power curtailed on an annual basis. TAC is estimated by addition of Annualized Capital Cost (ACC) and Annualized Replacement Cost (ARC) of battery bank and inverter.

On the one hand, ACC is calculated according to (14) [31] [32]:

$$ACC = (BCC + ICC)CRF(i, N_P), \tag{14}$$

where BCC is the battery bank capital cost, ICC is the inverter capital cost, i is the interest rate, N_P is the project lifetime, and $CRF(i, N)$ is the capital recovery factor considering interest rate i and time period N, as presented in (15):

$$CRF(i, N) = \frac{i(1+i)^N}{1+i^N-1}, \tag{15}$$

On the other hand, ARC is calculated according to (16) [31]-[32]:

$$ARC = (BRC)SFF(i, N_B) + (IRC)SFF(i, N_I), \tag{16}$$

where BRC is the battery bank replacement cost, IRC is the inverter replacement cost, N_B is the battery bank lifetime, N_I is inverter lifetime. $SFF(i, N)$ is the sinking fund factor for the interest rate i and time period N, being calculated according to (17):

$$SFF(i, N) = \frac{i}{1+i^N-1}, \tag{17}$$

Finally, TAC is calculated as the addition between ACC and ARC.

b) Battery bank lifetime

In the case of a storage system, battery bank lifetime is estimated by means of Ah throughput model, at which the energy available to be cycled over the battery lifetime remains constant without being affected by the depth of discharge of a determined cycle. Estimation of battery throughput (Q_b) is done by using Eq. 18 [33]:

$$Q_b = \frac{1}{T_b} \sum_{q=1}^{q=T_b} E_{max}(DOD_q)(CF_q), \quad (18)$$

This aging model requires using the curve that describes the behavior of number of cycles as a function of depth of discharge, found in Eq. 7 determined earlier. Under this context; in Eq. 16, E_{max} is the capacity of the battery bank, q *(q=1,...,T_b)* is the *q*th point of the discretized curve of number of cycles as a function of depth of discharge, while DOD_q and CF_q are depth of discharge and cycle of failure of the point q, respectively. In order to determine the storage system lifetime, the energy cycled by the battery is added; so that, when this value equals the expected lifetime Q_b, the lifetime of battery bank is finished. To consider feasible values of battery bank lifetime, those values obtained from the application of Ah throughput model are limited by the float lifetime of the battery bank provided by the manufacturers.

c) Case Study

In our case study, a technical-economic analysis was carried out by considering capital cost of the battery bank equal to 366 €/kW and the capital cost of inverter equal to 298 €/kWh; for simplicity, replacement costs were assumed to be equal to the capital cost, operation and maintenance costs were assumed to be 3.6 €/kW-year. Also, project lifetime was considered as 40 years, interest rate 8%, float lifetime of battery bank was assumed as 15 years, and power converter lifetime was considered as 20 years [19]. Using the aforementioned data in combination with the wind power curtailed obtained from computational simulations, the relationship between annualized cost and wind power curtailed was examined in order to select the appropriate size of the energy storage system. This relation is shown in Fig. 16 (scenario I); where the corresponding capacities of battery bank and power converter are presented as well. As can be observed, the point at which wind power curtailment and annualized cost are simultaneously reduced corresponds to the installation of a battery bank of 288 MWh/40 MW. As for the scenario II (Fig. 17) the optimal solution leads to the same result – using the same storage capacity, however providing a reduction of 13.2% on wind power curtailment compared to scenario I. The wind power curtailed in Scenario I is 69.34 GWh/yr and in Scenario II is 79.89 GWh/yr, while both are significantly better than without NaS storage support – 176.4 GWh/yr.

"See Fig. 16 at the end of the manuscript".

"See Fig. 17 at the end of the manuscript".

6. Conclusions

This paper explored wind curtailment mitigation effect by means of energy storage resources and Sodium/Sulfur (NaS) cell batteries. Due to its high level of renewable energy integration, Crete Island was used as a real case study where installed wind power capacity it is not fully explored. Constraints imposed by heavy steam turbines force periodic curtailment actions to preserve grid stability. Therefore, a time-shifting control strategy was employed to reduce wind curtailment. The control system allows NaS battery operation on a daily charging/discharging scheme, though was permitted only a full cycle per day. Curtailment mitigation performance was evaluated considering two time frame scenarios in order to shift wind generation to off-peak hours (Scenario I) and not only off-peak hours (Scenario II). Then, a technical-economic analysis for optimal sizing of the battery energy storage system was performed using as base criteria the total annualized cost of the storage system and the wind power curtailed on an annual basis. It was concluded that the point at which wind power curtailment and annualized cost are both reduced corresponded to the installation of a battery bank of 288 MWh/40 MW. As for the scenario II, the optimal solution leads to the same result. In the first scenario it was possible to recover circa 54.71 % of the initial estimated curtailment value for the studied year. On the other hand, by electing time shifting Scenario 2 it was possible to recover around 60.69%, which means that it was the best option since both scenarios costs are equal.

Acknowledgements

This work was supported by FEDER funds (European Union) through COMPETE and by Portuguese funds through FCT, under Projects FCOMP-01-0124-FEDER-020282 (Ref. PTDC/EEA-EEL/118519/2010) and UID/CEC/50021/2013. The research leading to these results has also received funding from the EU Seventh Framework Programme FP7/2007-2013 under grant agreement no. 309048.

References

[1] R. Komiyama, T. Otsuki and Y. Fujii, “Energy modeling and analysis for optimal grid integration of large-scale variable renewables using hydrogen storage in Japan,” *Energy,* vol. 81, pp. 537-555, 2015.

[2] E. Rodrigues, R. Godina, S. Santos, A. Bizuayehu, J. Contreras and J. Catalão, “Energy storage systems supporting increased penetration of renewables in islanded systems,” *Energy,* vol. 75, pp. 265-280, 2014.

[3] R. Edmunds, T. Cockerill, T. Foxon, D. Ingham and M. Pourkashanian, "Technical benefits of energy storage and electricity interconnections in future British power systems," *Energy,* vol. 70, pp. 577-587, 2014.

[4] K. Porter, J. Rogers and R. Wiser, "Update on Wind Curtailment in Europe and North America," 2011. [Online]. Available: http://www.efchina.org. [Accessed 2015].

[5] R. Wiser and M. Bolinger, "2013 Wind Technologies Market Report," U.S. Department of Energy, 2014.

[6] Y. Gu and L. Xie, "Fast Sensitivity Analysis Approach to Assessing Congestion Induced Wind Curtailment," *IEEE Transactions on Power Systems,* vol. 29, no. 1, pp. 101-110, 2014.

[7] X. Li, D. Hui and X. Lai, "Battery Energy Storage Station (BESS)-Based Smoothing Control of Photovoltaic (PV) and Wind Power Generation Fluctuations," *IEEE Transactions on Sustainable Energy,* vol. 4, no. 2, pp. 464-473, 2013.

[8] T. Brekken, A. Yokochi, A. von Jouanne, Z. Yen, H. Hapke and D. Halamay, "Optimal Energy Storage Sizing and Control for Wind Power Applications," *IEEE Transactions on Sustainable Energy,* vol. 2, no. 1, pp. 69-77, 2011.

[9] T.-C. Yang, "Initial study of using rechargeable batteries in wind power generation with variable speed induction generators," *IET Renewable Power Generation,* vol. 2, no. 2, pp. 89-101, 2008.

[10] R. L. Fares and M. E. Webber, "A flexible model for economic operational management of grid battery energy storage," *Energy,* vol. 78, p. 768–776, 2014.

[11] C. Murillo-Sanchez, R. Zimmerman, C. Lindsay Anderson and R. Thomas, "Secure planning and operations of systems with stochastic sources, energy storage, and active demand," *IEEE Transactions on Smart Grid,* vol. 4, no. 4, pp. 2220-2229, 2013.

[12] C. Colson, M. Nehrir, R. Sharma and B. Asghari, "Improving sustainability of hybrid energy systems part I: Incorporating battery round-trip efficiency and operational cost factors," *IEEE Transactions on Sustainable Energy,* vol. 5, no. 1, pp. 37-45, 2014.

[13] S. Tewari, "Chapter 3 - Potential of Sodium-Sulfur Battery Energy Storage to Enable Further Integration of Wind," in *In Energy Storage for Smart Grids*, P. D. Lu, Ed., Boston, Academic Press, 2015, pp. 67-95.

[14] S. Obara, Y. Morizane and J. Morel, "Economic efficiency of a renewable energy independent microgrid with energy storage by a sodium–sulfur battery or organic chemical hydride," *International Journal of Hydrogen Energy,* vol. 38, no. 21, pp. 8888-8902, 2013.

[15] P. Kou, F. Gao and X. Guan, "Stochastic predictive control of battery energy storage for wind farm dispatching: Using probabilistic wind power forecasts,," *Renewable Energy,* vol. 80, pp. 286-300, 2015.

[16] S. Carr, G. C. Premier, A. J. Guwy, R. M. Dinsdale and J. Maddy, "Energy storage for active network management on electricity distribution networks with wind power," *IET Renewable Power Generation,* vol. 8, no. 3, p. 249–259, 2014.

[17] S. Tewari and N. Mohan, "Value of NAS Energy Storage Toward Integrating Wind: Results From the Wind to Battery Project," *IEEE Transactions on Power Systems,* vol. 28, no. 1, pp. 532-541, 2013.

[18] M. Tahmasebi and J. Pasupuleti, "Self-Scheduling of Joint Wind Power and NaS Battery Plants in Spinning Reserve and Energy Markets," *Journal of Electrical Systems,* vol. 10, no. 2, pp. 156-167, 2014.

[19] B. Zakeri and S. Syri, "Electrical energy storage systems: A comparative life cycle cost analysis," *Renewable and Sustainable Energy Reviews,* vol. 42, p. 569–596, 2015.

[20] P. Haessig, B. Multon, H. Ben Ahmed, S. Lascaud and L. Jamy, "Aging-aware NaS battery model in a stochastic wind-storage simulation framework," in *2013 IEEE Grenoble PowerTech (POWERTECH)*, Grenoble, 2013.

[21] B. Polgari and B. Hartmann, "Energy storage for Hungary - NaS battery for wind farms," in *Proceedings of the 2011 3rd International Youth Conference on Energetics (IYCE)*, Leiria, 2011.

[22] D. Pavković, M. Hoić, J. Deur and J. Petrić, "Energy storage systems sizing study for a high-altitude wind energy application," *Energy,* vol. 76, pp. 91-103, 2014.

[23] SiNGULAR, "Smart and Sustainable Insular Electricity Grids Under Large-Scale Renewable Integration," Grant Agreement No: 309048, FP7-EU, 2015. [Online]. Available: http://www.singular-fp7.eu/home/. [Accessed 2015].

[24] C. Hansen and A. Papalexopoulos, "Operational impact and cost analysis of increasing wind generation in the island of Crete," *IEEE Systems Journal,* vol. 6, no. 2, pp. 287-295, 2012.

[25] Sandia National Laboratories, "NAS Battery Demonstration at American Electric Power: A Study for the DOE Energy Storage Program," March 2007. [Online]. Available: http://www.sandia.gov.. [Accessed 09 05 2015].

[26] M. Swierczynski, D. Stroe, A.-I. Stan, R. Teodorescu and D. Sauer, "Selection and performance-degradation modeling of LiMO2/Li4Ti5O12 and LiFePO4/C battery cells as suitable energy storage systems for grid integration with wind power plants: an example for the primary frequency regulation service," *IEEE Transactions on Sustainable Energy,* vol. 5, no. 1, pp. 90-101, 2014.

[27] H. L. Ferreira, R. Garde, G. Fulli, W. Kling and J. P. Lopes, "Characterisation of electrical energy storage technologies," *Energy,* vol. 53, pp. 288-298, 2013.

[28] Y. Shen, "Hybrid unscented particle filter based state-of-charge determination for lead-acid batteries," *Energy,* vol. 74, pp. 795-803, 2014.

[29] S. Li and B. Ke, "Study of battery modeling using mathematical and circuit oriented approaches," in *2011 IEEE Power and Energy Society General Meeting*, San Diego, CA, 2011.

[30] J. Guo, Z. Li and M. Pecht, "A Bayesian approach for Li-Ion battery capacity fade modeling and cycles to failure prognostics," *Journal of Power Sources,* vol. 281, pp. 173-184, 2015.

[31] T. Lambert, P. Gilman and P. Lilienthal, "Chapter 15. Micropower System Modeling with Homer," in *Integration of Alternative Sources of Energy*, F. A. Farret and G. Simões, Eds., John Wiley & Sons, Inc., 2006, pp. 379-418.

[32] H. Yang, Z. Wei and L. Chengzhi, "Optimal design and techno-economic analysis of a hybrid solar–wind power generation system," *Applied Energy,* vol. 86, no. 2, pp. 163-169, 2009.

[33] H. Bindner, T. Cronin, P. Lundsager, J. F. Manwell, U. Abdulwahid and I. Baring-Gould, "Lifetime Modelling of Lead Acid Batteries," Risø National Laboratory, Roskilde, 2005.

1
2
3

Figure captions

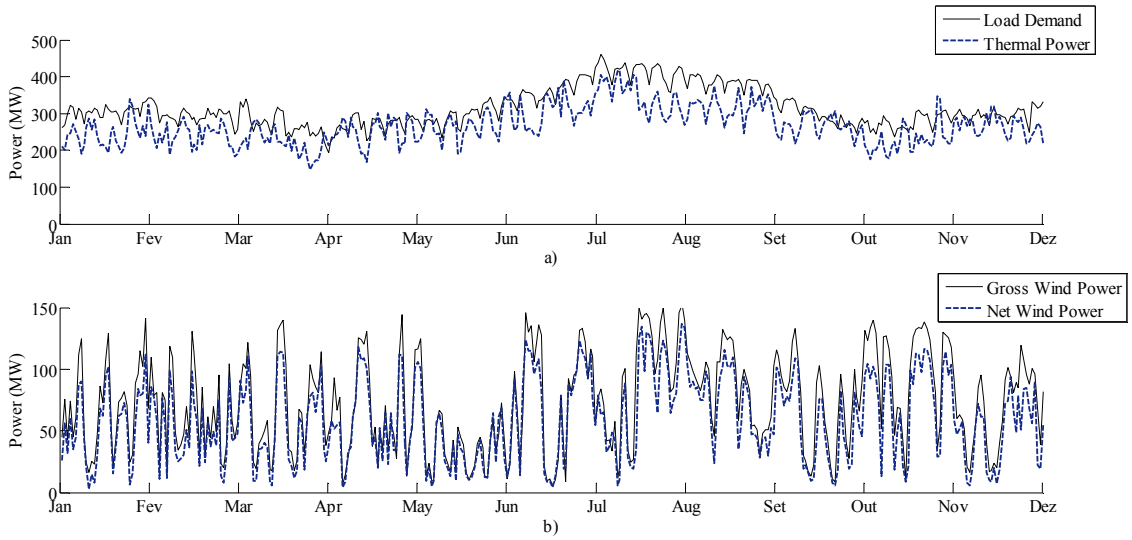

Fig. 1. Time series of Crete power grid: a) Load demand and thermal power generation; b) Gross and net wind power generation.

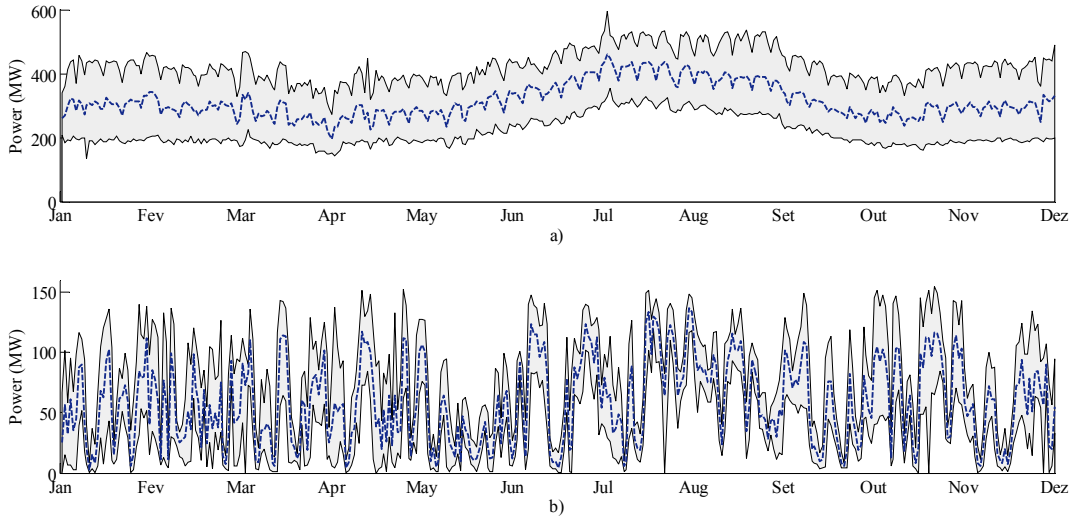

Fig. 2. Comparison of time series based on maximum, minimum and average values: a) Demand; b) Theoretical wind power generation.

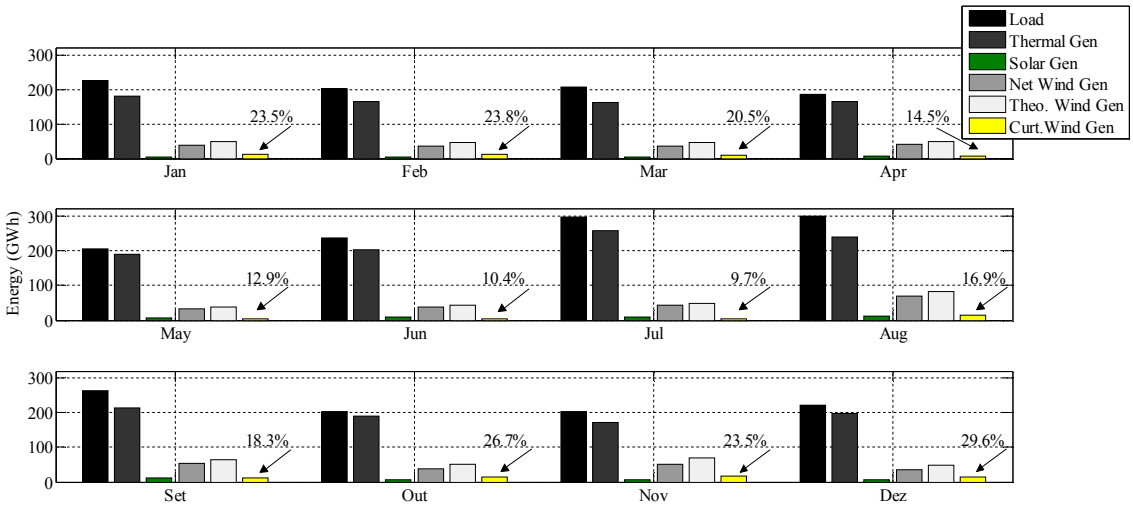

Fig. 3. Monthly generation levels for conventional and non-conventional plants versus consumption.

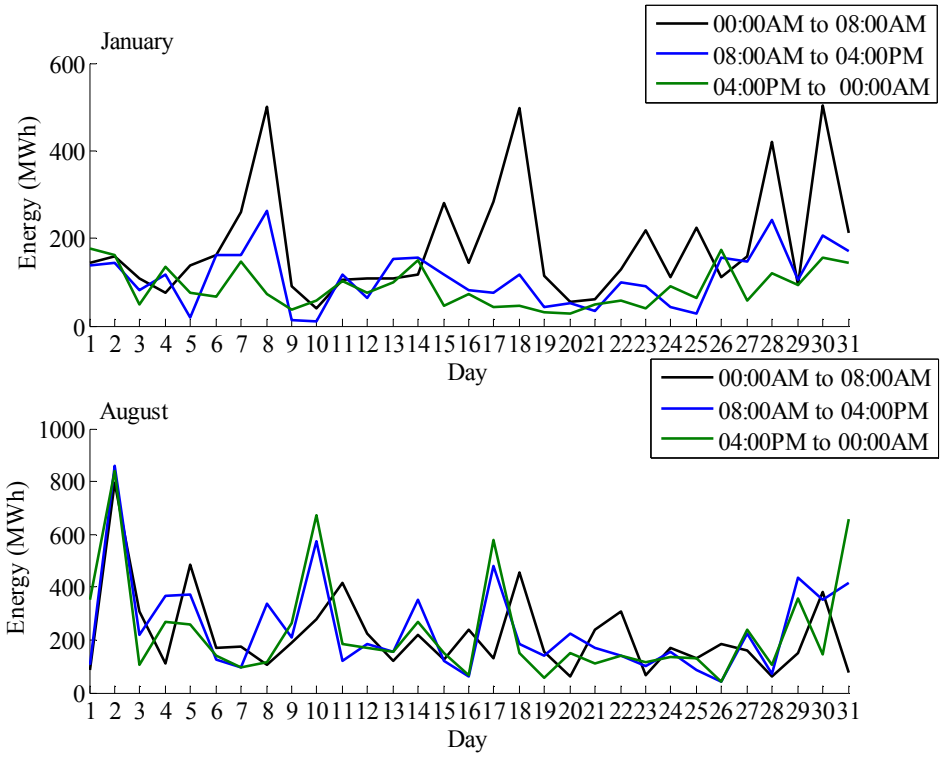

Fig. 4. Wind curtailment evolution for different periods of the day.

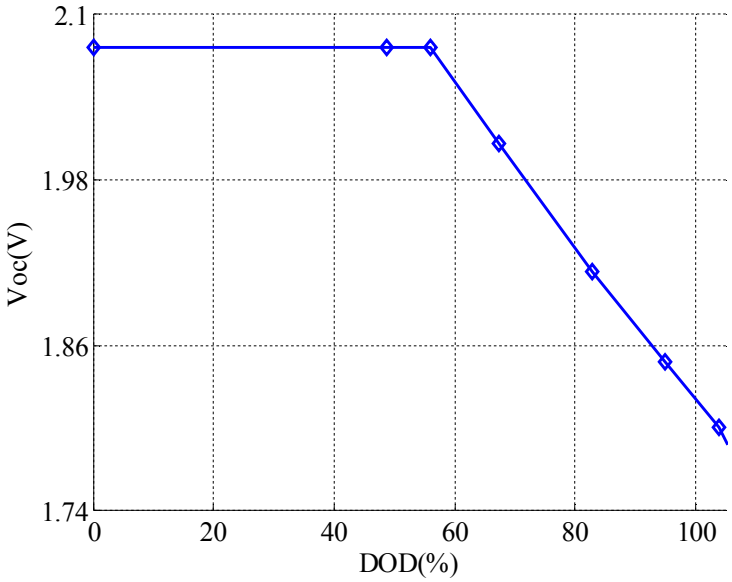

Fig. 5. Open circuit voltage as function of battery DOD.

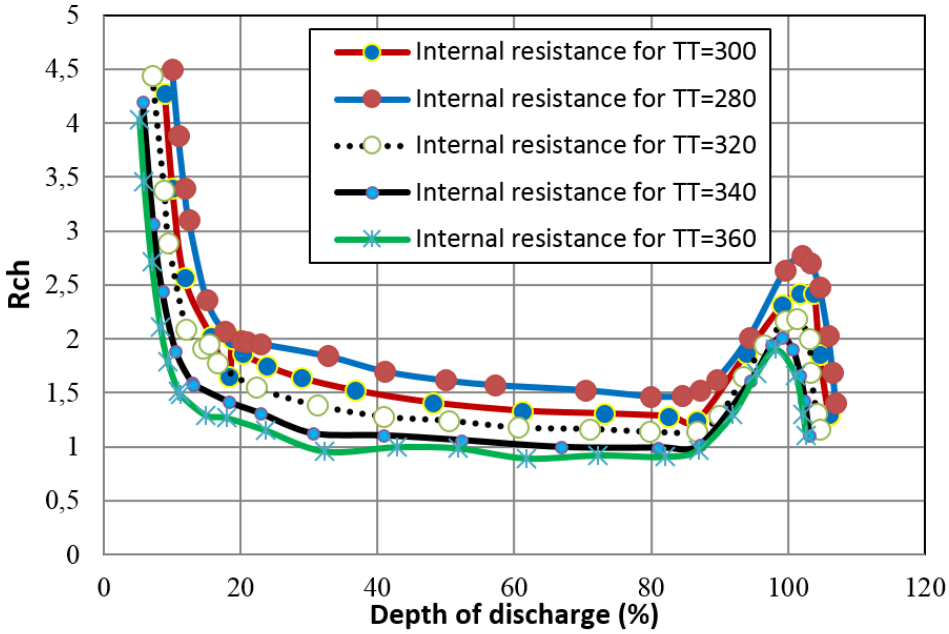

Fig. 6. NaS cell resistance in charging mode vs DOD at different temperatures.

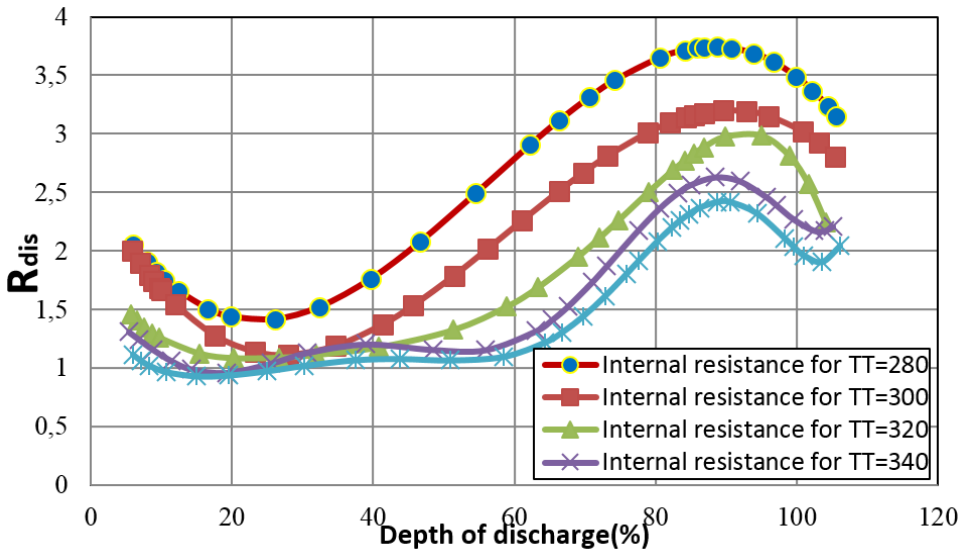

Fig. 7. NaS cell resistance in discharging mode vs DOD at different temperatures.

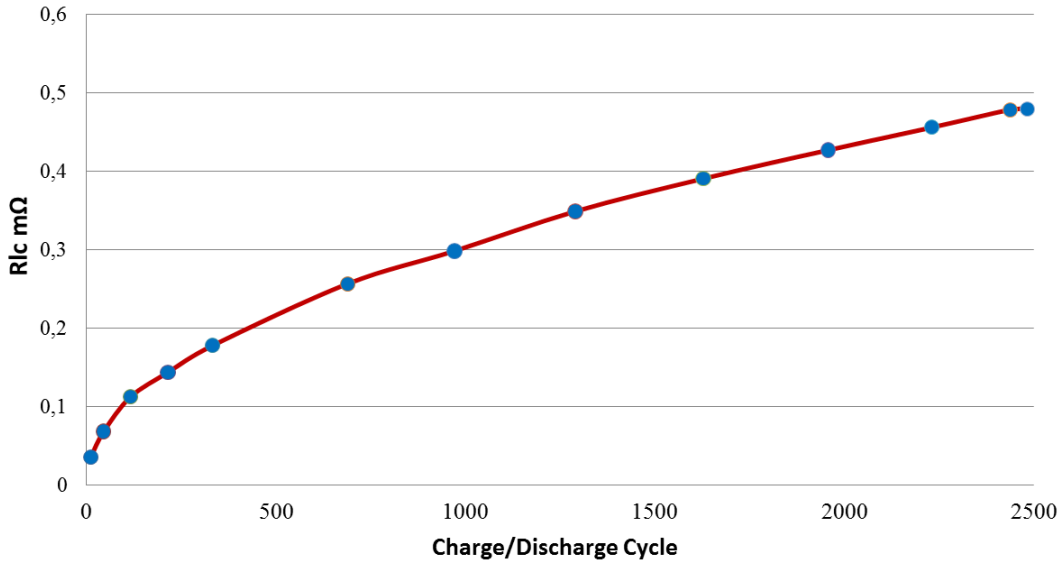

Fig. 8. Variation in internal resistance of NaS battery as a function of charge-discharge cycles.

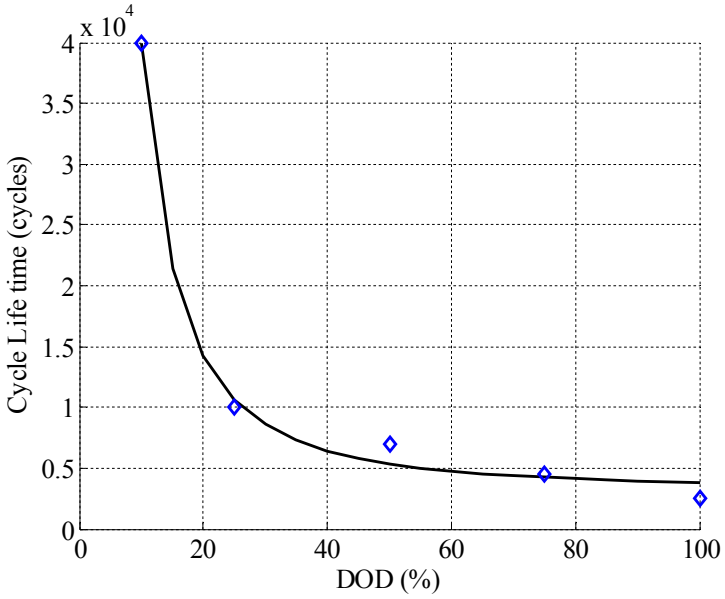

Fig. 9. Depth of discharge vs lifetime in cycles for NaS battery.

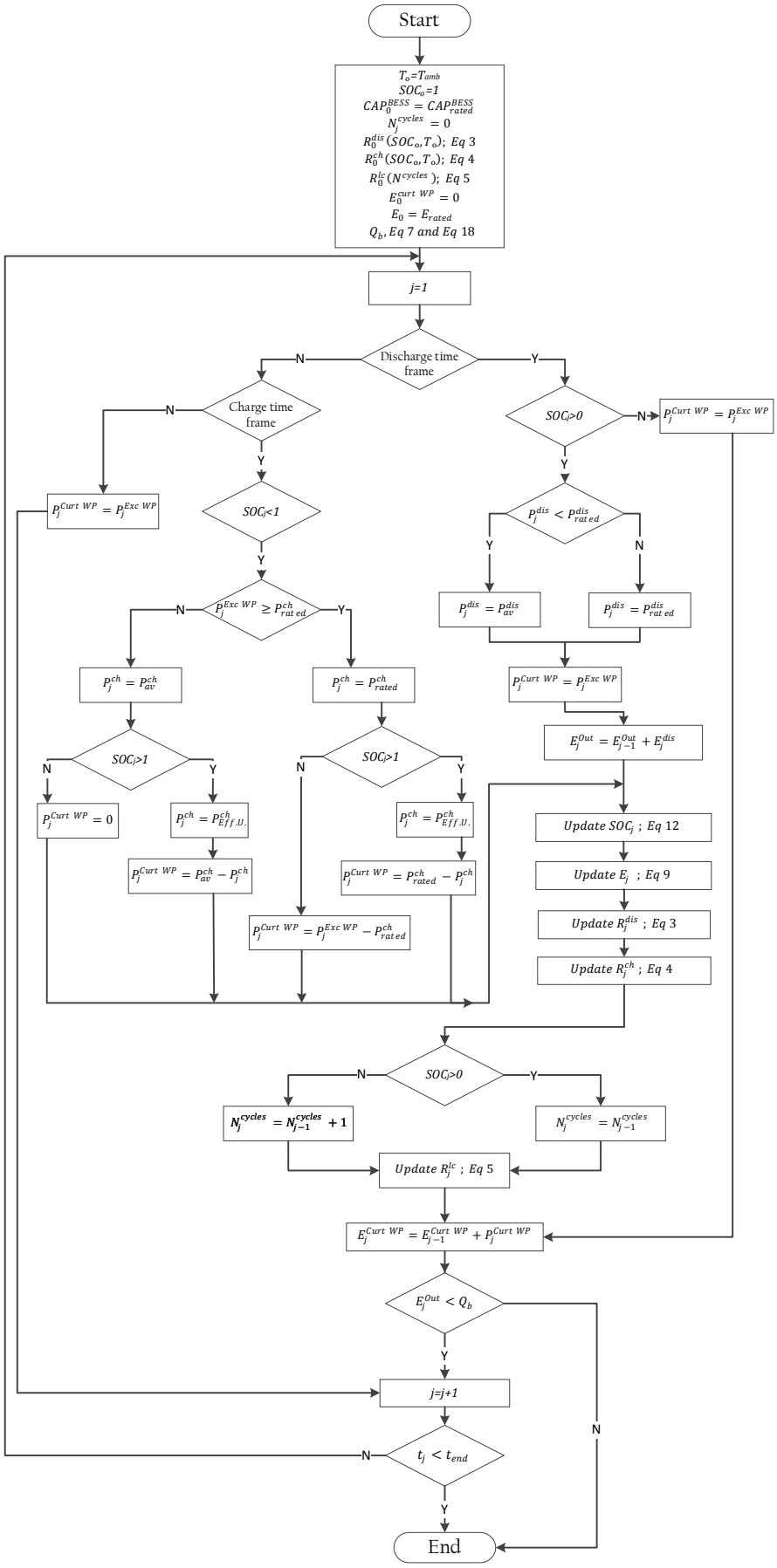

Fig. 10. Process flowchart

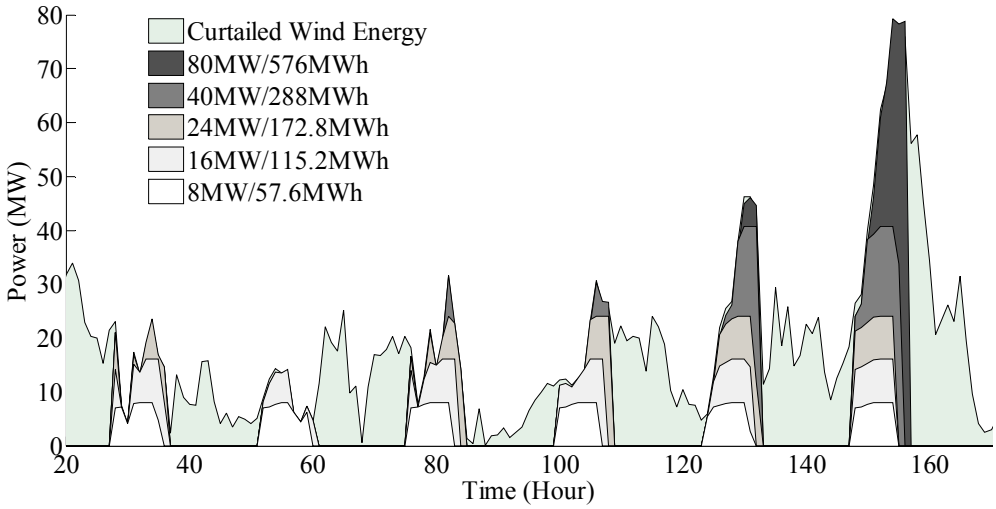

Fig. 11. Power to energy ratio effect on wind curtailment storage.

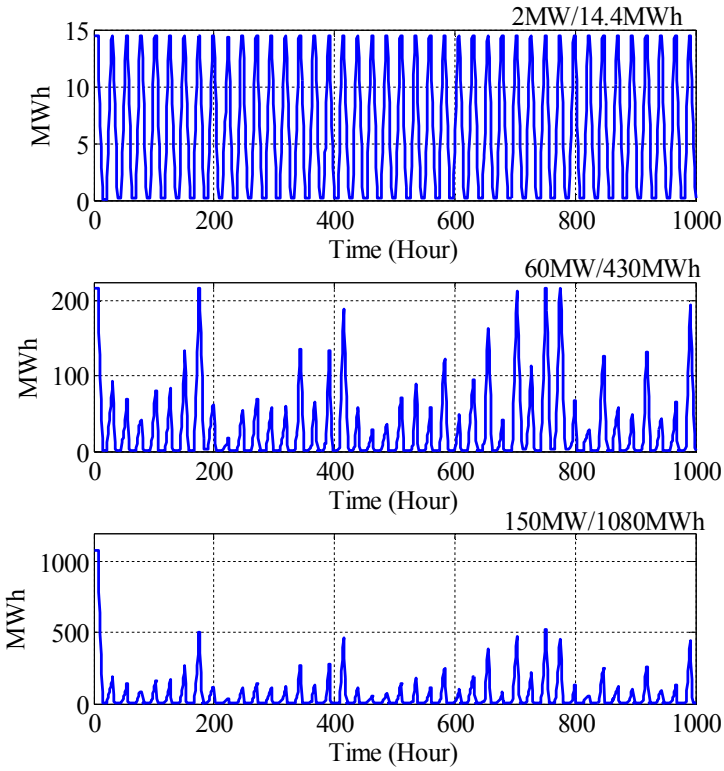

Fig. 12. State of charge profile at daily operation.

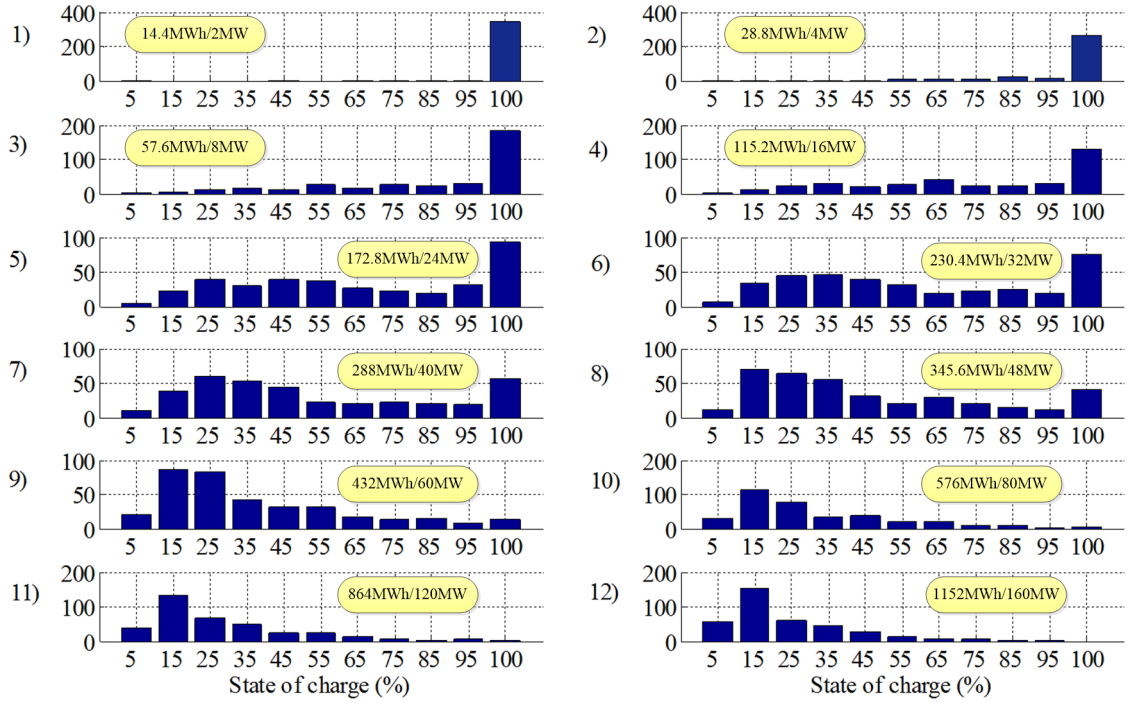

Fig. 13. DOD distribution for one year of operation as function of battery bank size.

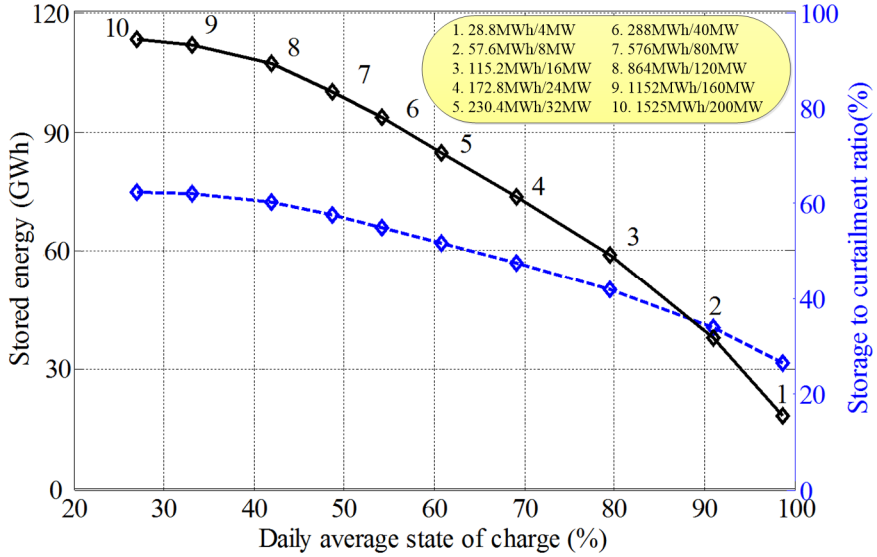

Fig. 14. NaS battery storage system performance (Scenario I).

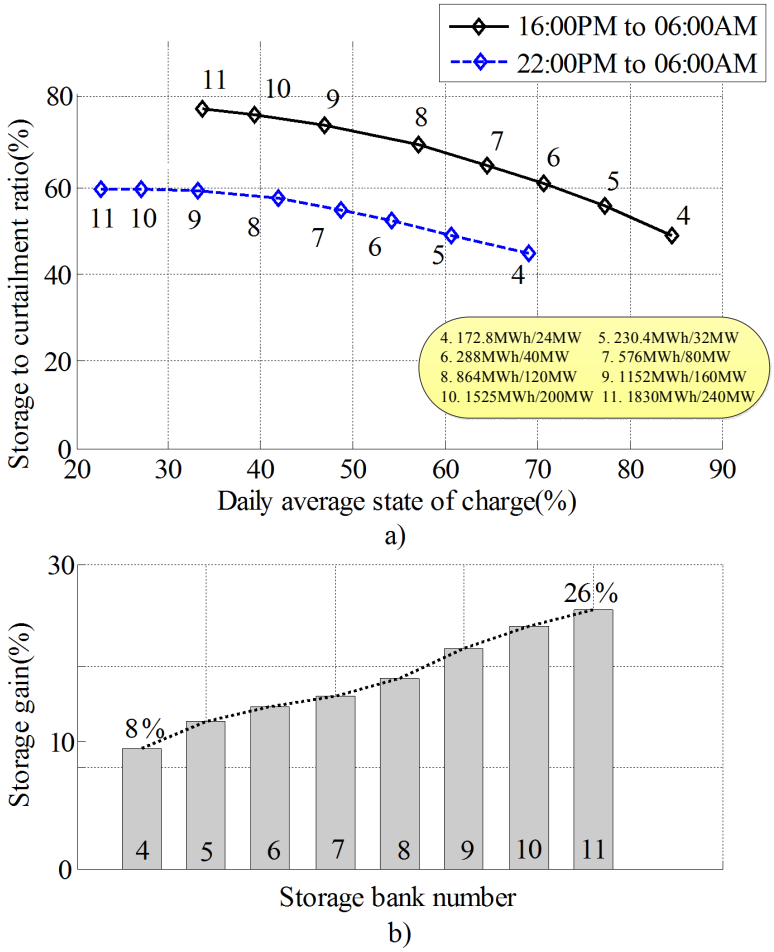

Fig. 15. Performance comparison between scenarios I and II.

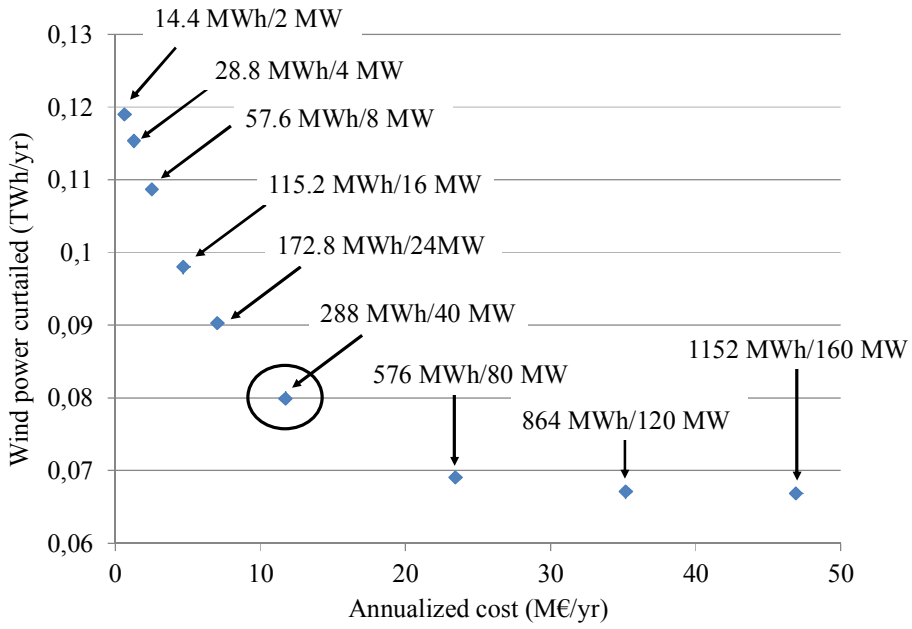

Fig. 16. Scenario I: Annualized cost vs. Wind power curtailment.

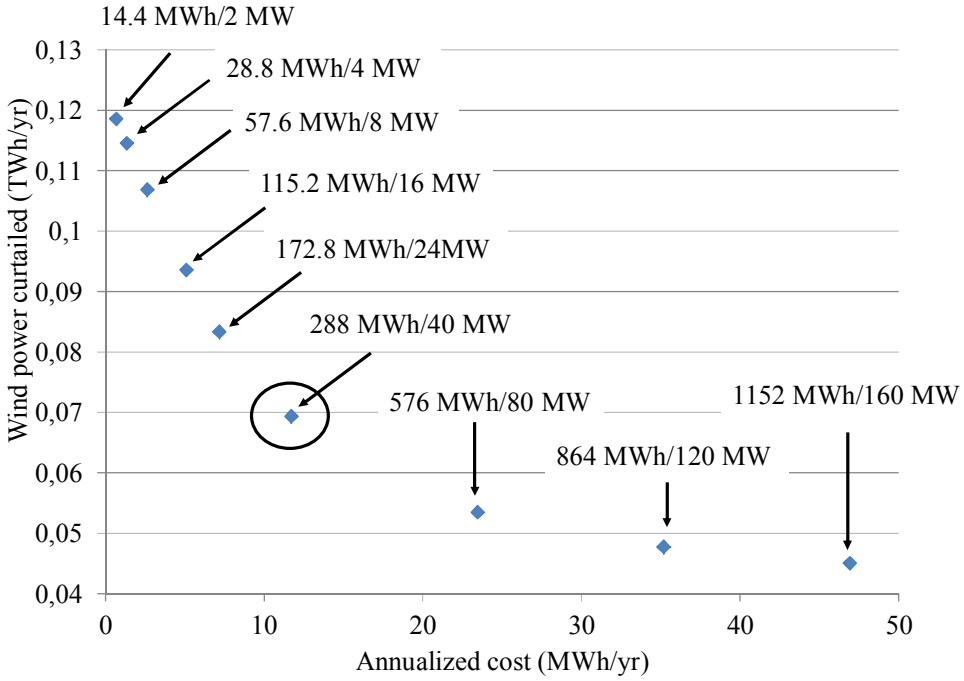

Fig. 17. Scenario II: Annualized cost vs. Wind power curtailment.

Tables

Table 1 – R_{ch} curve fit coefficients.

T(ºC)	a	b	c	d	e	f	g	h	i	j
360	1,48E+01	-3,603443562	4,00E-01	-2,41E-02	8,70E-04	-1,96E-05	2,76E-07	-2,38E-09	1,14E-11	-2,34E-14
340	20,11296449	-4,387864529	0,447506939	-0,02529688	0,000867232	-1,87394E-05	2,56423E-07	-2,15338E-09	1,01172E-11	-2,03428E-14
320	2,01E+01	-4,387864529	4,48E-01	-2,53E-02	8,67E-04	-1,87E-05	2,56E-07	-2,15E-09	1,01E-11	-2,03E-14
300	2,95E+01	-6,366800815	6,23E-01	-0,033715155	1,11E-03	-2,31952E-05	3,08E-07	-2,51496E-09	1,15E-11	-2,26649E-14
280	3,35E+01	-6,547631017	5,79E-01	-0,028617152	8,73E-04	-1,70977E-05	2,16E-07	-1,70125E-09	7,60E-12	-1,46673E-14

Table 2– R_{dis} curve fit coefficients.

T(ºC)	a	b	c	d	e	f	g	h	i
360	1,69E+00	-1,61E-01	1,45E-02	-7,53E-04	2,52E-05	-5,29E-07	6,52E-09	-4,24E-11	1,11E-13
340	1,451739659	0,005037734	-0,009187198	0,00072225	-2,2882E-05	3,51828E-07	-2,5947E-09	7,34538E-12	
320	1,94274868	-0,115341762	0,005817645	-0,000139602	1,63197E-06	-6,94486E-09			
300	2,612556873	-0,122419802	0,002916653	-1,64878E-05					
280	2,601052094	-0,110064786	0,002933269	-1,74444E-05					